MOX-Report No. 82/2023

Geometric control by active mechanics of epithelial gap closure

Pozzi, G.; Ciarletta, P.

MOX, Dipartimento di Matematica
Politecnico di Milano, Via Bonardi 9 - 20133 Milano (Italy)

mox-dmat@polimi.it https://mox.polimi.it

Geometric control by active mechanics of epithelial gap closure.

G. Pozzi[1*], P. Ciarletta[1†]

[1] MOX, Dipartimento di Matematica, Politecnico di Milano,

piazza Leonardo da Vinci 32, 20133 Milano, Italy.

Abstract

Epithelial wound healing is one of the most important biological processes occurring during the lifetime of an organism. It is a self-repair mechanism closing wounds or gaps within tissues to restore their functional integrity. In this work we derive a new diffuse interface approach for modelling the gap closure by means of a variational principle in the framework of non-equilibrium thermodynamics. We investigate the interplay between the crawling with lamellipodia protrusions and the supracellular tension exerted by the actomyosin cable on the closure dynamics. These active features are modeled as Korteweg forces into a generalised chemical potential. From an asymptotic analysis, we drive a pressure jump across the gap edge in the sharp interface limit. Moreover, the chemical potential diffuses as a Mullins-Sekerka system, and its interfacial value is given by a Gibbs-Thompson relation for its local potential driven by the curvature-dependent purse-string tension. The Finite Element simulations show an excellent quantitative agreement between the closing dynamics and the morphology of the edge with respect to existing biological experiments. The resulting force patterns are also in good qualitative agreement with existing traction force microscopy measurements. Our results shed light on the geometrical control of the gap closure dynamics resulting from the active forces that are chemically activated around the gap edge.

Keywords wound healing, diffuse interface, purse-string, crawling, Cahn-Hilliard-Brinkman, Mullins-Sekerka.

*Author current affiliation: DISMA, Politecnico di Torino, corso Duca degli Abruzzi 24, 10129 Torino, Italy

†Corresponding author. E-mail: pasquale.ciarletta@polimi.it

Introduction

Living tissues have the ability to self-repair in response to injury by closing wound and gaps through a series of coordinated cellular and supracellular processes. Wounds may not only result from surgery or accidental trauma, but also from pathological conditions, such as cancer, diabetes or inflammatory processes. Moreover, it is known that a dysregulation of the physiological features of wound healing could result in severe infection and it can itself promote the onset of cancer [1].

Wound healing keeps attracting a lot of interest in soft matter physics [2].

Early surgical data reported a linear decay of the radius of a circular wound over time in mammalians [3]. Sherratt and Murray [4–6] fitted this experimental trend using a model that only accounts for either an activator or an inhibitor of mitosis produced by epidermal cells in the healing process. Thus, they somewhat supported the view that biochemical control of mitosis plays a major role in re-epithelialization [7].

However, many *in-vivo* and *in-vitro* experiments performed during the last decades pointed out the key role of a coordinated movement of epithelial cells to close the wound and re-establish tissue integrity for both embryonic and adult skin layers. Thus, several modelling approaches have been recently to elucidate the key mechano-biological features at play.

If epidermal cells are not motile in physiologic condition, it has been found that they undergo a marked phenotype alteration in the neighborhood of the wound, acquiring the ability to crawl via lamellipodia protrusions, [8]. Conversely, embryonic epidermal movement was found to be triggered by a circumferential tension at the free edge, acting like a purse string pulling [9].

Wounds induced in Madin–Darby canine kidney epithelial cell monolayers were found to close by a crawling behavior involving Rac, phosphoinositides and active movement of multiple rows of cells, while active actin bundles were not found to be necessary for closing, yet playing a role in determining the regularity of closure [10]. Moreover, specific signaling pathways were identified to control both such mechanical features for the dorsal wound closure in the drosophila embryos [11].

Later studies revealed that the wound closure is driven simultaneously by the cells active crawling on the substrate through lamellipodia and the constriction by a supracellular actomyosin cable, referred as purse-string mechanism [12, 13]. However, even if these processes are not mutually exclusive, their coexistence is strongly influenced by the surrounding environment and by chemical factors [14]. Cells

indeed develop cytoskeletal protrusions (i.e. lamellipodia) in epithelia with abundant extracellular matrix (ECM) to spread over a substrate [15]. An actomyosin supracellular structure, able to generate actively contractile mechanical forces, was instead the dominant mechanism found in other system models, either in presence of apoptotic cells [9] or in epithelia lacking ECM [16]. Moreover, traction force patterns at later stages of wound healing pointed out the existence of tensions transmitted by the actomyosin ring to the underlying substrate through focal adhesions [17, 18].

The mechano-biological coupling between the crawling and the purse-string mechanism has been proven to be regulated by the curvature of the wound edge [19, 20] and by the substrate stiffness [21].

Several mathematical approaches have been proposed to characterize such a complex interplay of geometrical and mechanical feature in wound healing. A level-set model has been proposed to describe the edge motion regulated by cell mitosis and lamellipodia-induced migration, also accounting for the reaction diffusion dynamics of the epidermal growth factor [22]. A continuous approach described the effect of the purse-string mechanisms as contraction of the healthy tissue surrounding the wound governed by the momentum balance equation and the mutual signaling among cells [23]. Other continuous approaches considered the balance of forces acting on a single cell embedded in an epithelial monolayer, showing that single cell crawling is sufficient to drive the collective motion of a cells layer by means of cell-cell adhesion [24–26]. The combined effect of crawling and purse string was investigated in [19] by a free boundary model of cell flowing as a viscous fluid subjected to localised forces at the moving edge. Crawling anD purse-string are therefore considered as source terms in the momentum balance at the edge boundary, posing important challenges for the numerical discretization and the mathematical well-posedness at late stages of gap closure.

Alternatively, discrete modelling approaches were proposed to investigate the traction force patterns exerted by the cells during the wound closure, by means of both vertex and Voronoi models [17, 27–30].

In this work, we propose a diffuse interface approach with the aim both to provide a suitable thermodynamic framework to characterize the evolution of the state variables driving the mechano-biologic coupling and to implement a robust yest computationally affordable numerical framework to simulate gap closure for any initial geometry. In contrast to existing sharp interface models, that require additional regularity requirements and compatibility equations for the motion of the free-boundary, here the motion of the diffuse interface is intrinsically driven by the evolution of a chemo-mechanical potential, driving a phase transition similarly to a Gibbs potential in supercooling. Phase-field approaches have

been successfully proposed for describing both individual and collective cell migration in tissue monolayers [31–33]. Here, beyond the state-of-the-art, we consider epithelial wound healing as a non-equilibrium system whose evolution is governed by irreversible mass and energy flows. By introducing appropriate non-equilibrium state variables, we derive from mixture theory a diffuse interface model for the healing process that incorporates the crawling and the purse-string mechanisms in the free energy. Our modeling choice notably allows to overcome the numerical difficulties to model the motion of the sharp-interface through forces dependent on geometric properties of the free-boundary, such as the local curvature. Thus, the proposed model aims to bridge the gap between the tissue and the cellular scales by accounting for the mechanisms of the lower scales in the form of a chemical potential at the mesoscale.

In what follows, we exploit formal asymptotic analysis to highlighting how the crawling, the purse-string mechanism at the wound edge and the friction with the substrate cooperate in regulating the wound closure process.. Finally, we present Finite Element simulations to validate the model results against the existing experimental data, discussing the predictions against the evolutoin over time of the wounded area, the morphological transitions at the edge and the generated traction patterns with the substrate.

Results

The diffuse interface model

We consider a simple system model made by a confluent monolayer of epithelial cells immersed in a large bath, where a gap is created by positioning a stencil of well-defined geometry in its center, as in [19]. Under the hypothesis of neglecting the fast-scale dynamics of calcium and myosin traveling from the periphery to the wound [34], we model the monolayer as a biphasic mixture with a diffuse interface that separates the wound from the healthy surrounding epithelial tissue. The variable $\phi(\mathbf{x}, t)$ describes the relative volume fraction of the wound with respect to the healthy phase in the mixture, and it is defined in such a way that $\phi = \{1\}$ in the wound area and $\phi = \{-1\}$ on the healthy tissue. The evolution of ϕ is partly driven by a gradient flow dependence with respect to a chemical potential μ, accounting for both the local interaction among cells by the derivative of a free energy double-well potential, $\Psi(\phi)$ and a short-range nonlocal interaction at the interface expressed by a gradient dependence [35, 36]. By following thermodynamics arguments and exploiting the maximum dissipation principle [37] (see Supplementary

Section 1 for model derivation), the evolution of the wounded monolayer is described by

$$\frac{\partial \phi}{\partial t} + \mathbf{u} \cdot \nabla \phi = -\Gamma + M \Delta \mu, \tag{1}$$

$$\mu = \frac{\beta}{\epsilon} \Psi'(\phi) - \beta \epsilon \Delta \phi, \tag{2}$$

where Γ and M are a crawling rate and a motility parameter, respectively, the parameter β plays the role of a surface tension at the wound edge, whereas ϵ is a measure of the interface thickness and $\mathbf{u}$ is the volume-averaged velocity of the mixture. The momentum balance equation

$$-\nabla \cdot \sigma + \eta \mathbf{u} = (\mu + f_L) \nabla \phi, \tag{3}$$

results in a Darcy-Brinkman equation, where the stress tensor σ is given by $= 2\nu \mathcal{D}(\mathbf{u}) - p\mathbb{I}$, being ν the viscosity of the mixture, $\mathcal{D}(\mathbf{u}) = 1/2(\nabla \mathbf{u} + \nabla \mathbf{u}^{\mathbf{T}})$ the symmetric part of the velocity gradient, p the hydrostatic pressure and $\mathbb{I}$ the identity matrix. In Eq. (3), the cell–cell forces are balanced by cell–substrate friction, given by a friction coefficient η, by the Korteweg forces exerted by the chemical potential μ, and by the active crawling potential f_L of the cellular lamellipodia. Overall, the mechanical forces exerted by the actomyosin cables are described as a surface tension at the wound edge in the chemical potential term μ through the parameter β. The cell crawling mechanism is also accounted introducing an extra chemical potential f_L, that results in a Korteweg force in the momentum balance equation, and a source term Γ representing the local crawling rate of the cellular phase over the wound. In the present set-up, the velocity is assumed to be solenoidal, and thus

$$\nabla \cdot \mathbf{u} = 0, \tag{4}$$

holds. At the border of the monolayer, assuming that the wound is sufficiently far from it, we impose the following no-flux boundary conditions:

$$\nabla \phi \cdot \mathbf{n} = 0, \qquad \nabla \mu \cdot \mathbf{n} = 0, \qquad \sigma \mathbf{n} = 0,$$

where $\mathbf{n}$ is the normal unit vector on the boundary, pointing towards the exterior of the monolayer.

Asymptotic Limit

To clarify better how crawling, purse-string mechanisms and friction with the substrate are embedded in the proposed model, we exploit a formal asymptotic analysis [38–43] on the model in the limit of zero thickness interface, i.e. taking $\epsilon \to 0$. We proceed by subdividing the wounded monolayer in two distinct parts: a slender area including the diffuse interface, which is called the *inner* region, and the union of the two not connected remaining portion of the monolayer, named as *outer* region, as sketched in Fig. 1 . Hence, we identify:

$$\Omega^+ = \{x \in \Omega : \phi_0(x) = +1\}, \qquad \Omega^- = \{x \in \Omega : \phi_0(x) = -1\},$$

as the two external subdomains representing the wound and the healthy tissue, respectively. Let us now denote by Σ_0 the limiting interface as the zero level sets of the variable ϕ. After performing the asymptotic expansions in the infinitesimal interface thickness ϵ for each variable in both the *outer* and the *inner* region, we match the *inner* and the *outer* solutions by imposing the compatibility conditions at the interface.

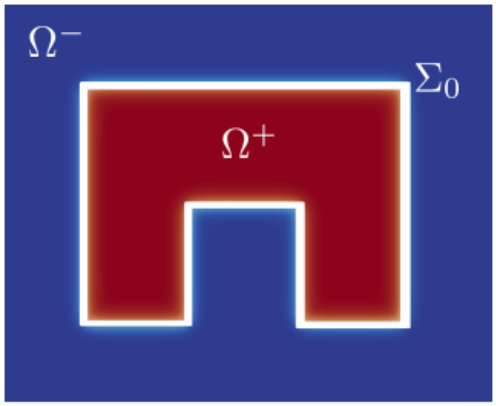

Figure 1: Sketch of the domain subdivided in *inner* and *outer* regions. The inner region is a narrow portion of thickness ϵ across the interface Σ_0 between the healthy and the wounded epithelium, characterised by a fast variation of the variable ϕ. The outer region is the union of the two non-connected bulk regions, $\Omega^+ \cup \Omega^-$. The total domain is a square of length L_c.

Following this procedure (for more details see Supplementary Section 2) we derive the correspondent

sharp interface limit model

$$\begin{cases} M\Delta(\mu_0) = \Gamma & \text{on } \Omega^+ \cup \Omega^-, \\ -2\nu\nabla\cdot\mathcal{D}(\mathbf{u}_0) + \eta\mathbf{u}_0 = -\nabla p_0 & \text{on } \Omega^+ \cup \Omega^-, \\ \nabla\cdot\mathbf{u}_0 = 0 & \text{on } \Omega^+ \cup \Omega^-, \end{cases} \tag{5}$$

on the wounded monolayer, referred to as on $\Omega^+ \cup \Omega^-$, excluding the interface between the healthy tissue and the wound, Σ_0. The system is complemented by the following jump conditions at Σ_0

$$[\mathbf{u}_0]^+_- \cdot \mathbf{n} = 0, \qquad [p_0]^+_- = 2(\mu_0 + f_L) \qquad \text{on } \Sigma_0, \tag{6}$$

$$[\mu_0]^+_- = 0, \qquad 2\mu_0 = \beta\kappa\frac{2\sqrt{2}}{3} \qquad \text{on } \Sigma_0, \tag{7}$$

$$2(-\mathcal{V} + u_{n,0}) = M[\nabla\mu_0]^+_- \cdot \mathbf{n} \qquad \text{on } \Sigma_0. \tag{8}$$

where κ and $\mathcal{V}$ are the local curvature and the normal velocity of the interface, respectively. Being f the generic variable of the diffuse interface model, here with f_0 we denote the principal component of the asymptotic outer expansion and with symbol $[f]^+_-$ we denote the jump of f at the interface.

In the sharp interface limit, we find that the mixture behaves as an incompressible Darcy-Brinkman fluid with two interfacial forces, corresponding to a normal crawling pressure with magnitude f_L and an active purse-string tension with characteristic force per unit length β. The movement of the interface is driven by a Mullins-Sekerka problem, where Γ defines the crawling energy source for the chemical potential. In physical terms, the purse-string mechanism lets the interface carry a chemical potential which results in an active surface tension β as given by the Gibbs-Thompson condition in Equation (7), and a friction with the substrate inversely proportional to the mobility parameter M as given by the Stefan condition in Equation (8).

Finite Element simulations

Before implementing the numerical approximation of the model, we derive its dimensionless version to identify the reduced set of dimensionless parameters governing the evolution of the biological system. To this purpose, we set a characteristic length-scale as the domain size L_c, a characteristic time-scale T_c

and a characteristic velocity $\mathbf{U}_c$. We thus introduce the dimensionless variables $\hat{x} = x/L_c$, $\hat{t} = t/T_c$ and $\hat{\mathbf{u}} = \mathbf{u}/U_c$ for space, time and velocity, respectively. We adopt the symbol $\hat{\nabla}$ to denote the dimensionless differential operators. Standard manipulations of the diffuse interface model lead to

$$\begin{cases} \frac{\partial \phi}{\partial \hat{t}} + \hat{\mathbf{u}} \cdot \hat{\nabla}\phi = -\bar{\Gamma} + \bar{M}\hat{\Delta}\hat{\mu}, \\ \hat{\mu} = \frac{1}{\bar{\epsilon}}\Psi'(\phi) - \bar{\epsilon}\hat{\Delta}\phi, \\ -Da\hat{\nabla} \cdot \mathcal{D}(\hat{\mathbf{u}}) + \hat{\mathbf{u}} = -\hat{\nabla}\hat{p} + (\hat{\mu} + \bar{f}_L)\hat{\nabla}\phi, \\ \hat{\nabla} \cdot \hat{\mathbf{u}} = 0 \end{cases} \tag{9}$$

and thus we identify five dimensionless parameters

$$\bar{\Gamma} = \frac{\Gamma \eta L_c^3}{\beta}, \qquad Da = \frac{\nu}{\eta L_c^2}, \qquad \bar{\epsilon} = \frac{\epsilon}{L_c}, \qquad \bar{M} = M\eta, \qquad \bar{f}_L = \frac{f_L L_c}{\beta},$$

having imposed the fundamental scaling $\beta/(L_c^2 U_c \eta) = 1$, so that the characteristic stress is $P_c = \eta L_c U_C = \beta/L_C$. Thus, $\hat{p} = p/P_c$ and $\hat{\mu} = \mu/P_c$, and the characteristic time is $T_c = L_C/U_C = \eta L_c^3/\beta$, i.e. the time at which frictional forces with the substrate are of the same order as the surface tension. The dimensionless parameter Da is the classical Darcy parameter for the Brinkman equation, i.e. the ratio between viscous and friction forces, $\bar{\Gamma}$ is the product between the crawling rate and the characteristic time, $\bar{\epsilon}$ is the ratio between the interface and domain sizes, $\bar{M}$ is the ratio between the viscous and the friction forces, and $\bar{f}_L$ is the ratio between crawling and purse string forces.

We performed numerical simulation on a square domain with unit dimensionless side, subdivided in $3.2 \cdot 10^5$ uniformly distributed triangles and we fix the characteristic length $L_c = 2.24 \cdot 10^{-4}$ m to reproduce *in-silico* the experimental system adopted by Ravasio et al. in [19]. We explore three different scenarios on varying the initial shape of the wound: in particular we chose the three initial gap configurations shown in Figure 2 (left), referred to as *square inset*, *half moon* and *half circle*. In every test case the initial area is about 4000 - 5000 µm^2. The numerical simulations are obtained using the library FEniCS for solving partial differential equations using Finite Element methods [44, 45].

In order to reproduce the experimental trends presented in [19], for all the three scenarios described above we found the values of the physical parameters from the literature, where present, by varying them in their physiological range and by defining as optimal set of parameters that better fit the area decay in

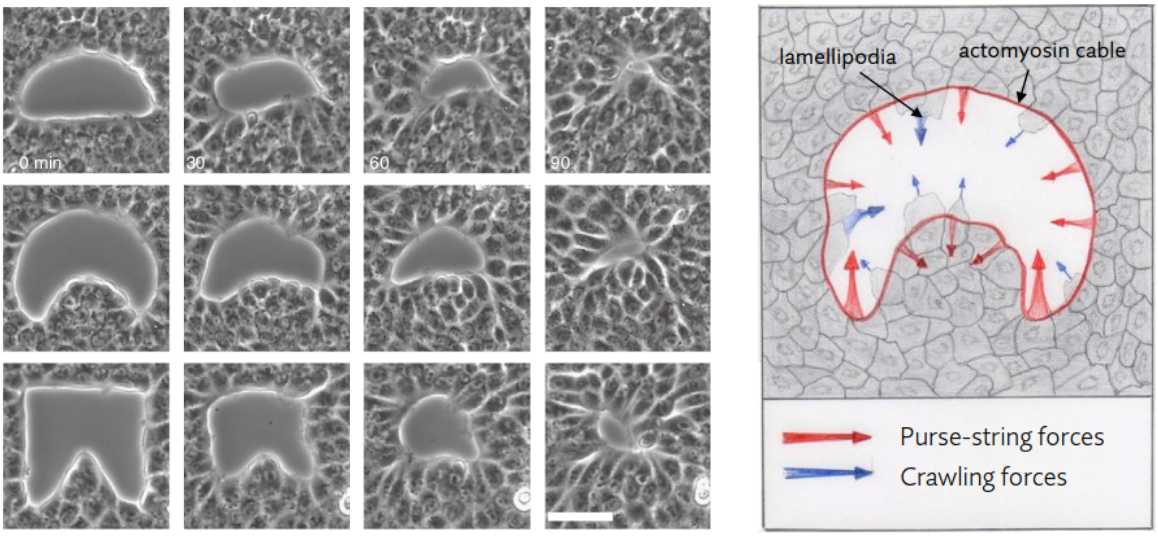

Figure 2: (Left) Example time lapses of gap closure. Scale bar 50 mm. (Right) Mechanical coupling between purse-string and crawling. Red and blue arrows indicate the direction of the local forces induced by purse-string and crawling, respectively. Image adapted from Ref. [19].

time. Thus, we set $f_L = 100\,\mathrm{Pa}$ [17, 24], $M = 3.27 \cdot 10^{-15}\,\mathrm{m^2\,Pa^{-1}\,s^{-1}}$ [36], $\nu = 6.0 \cdot 10^{7}\,\mathrm{Pa\,s}$ [46] while $\epsilon = 5 \cdot 10^{-7}\,\mathrm{m}$ is prescribed by the spatial scale of the problem. Finally, we calibrate $\beta = 4 \cdot 10^{-3}\,\mathrm{Pa\,m}$, $\eta = 3.09 \cdot 10^{5}\,\mathrm{Pa\,s\,m^{-2}}$ and $\Gamma = 5.62 \cdot 10^{-5}\,\mathrm{s^{-1}}$ to reproduce the experimental trends. Consequently, the dimensionless groups take the following values: $Da = 3.87 \cdot 10^{9}$, $\bar{\epsilon} = 2.23 \cdot 10^{-3}$, $\bar{\Gamma} = 4.88 \cdot 10^{-5}$, $\bar{M} = 1.01 \cdot 10^{-9}$ and $\bar{f}_L = 5.6$. The Finite Element discretization of the system (9) is discussed in the Supplementary Section 3.

As shown in Fig.3, the evolution is characterized by a common trend in the local regulation of the closure mechanism. In accordance with the experimental observations in [19], flat and negative curved edges, i.e. the ones protruding into the wound, advance at a considerably slower pace compared with boundary regions characterized by the presence of positive curvatures, see Fig. 4. Indeed, the early stage of the simulations consists in a regularization of the wound shape due to purse-string tension as observed by [18]. When the wound reaches a rounded shape and hence the whole border of the gap has positive curvature, each portion of the boundary moves with the same speed towards the center of the gap, up to the closure of the wound. This behavior, overlooking the initial shape of the wound, highlights the importance of the sign and the magnitude of the local curvature in governing the closure dynamics.

The *in-silico* healing times are approximately $40 - 60\,\mathrm{min}$, depending on the initial extension of the

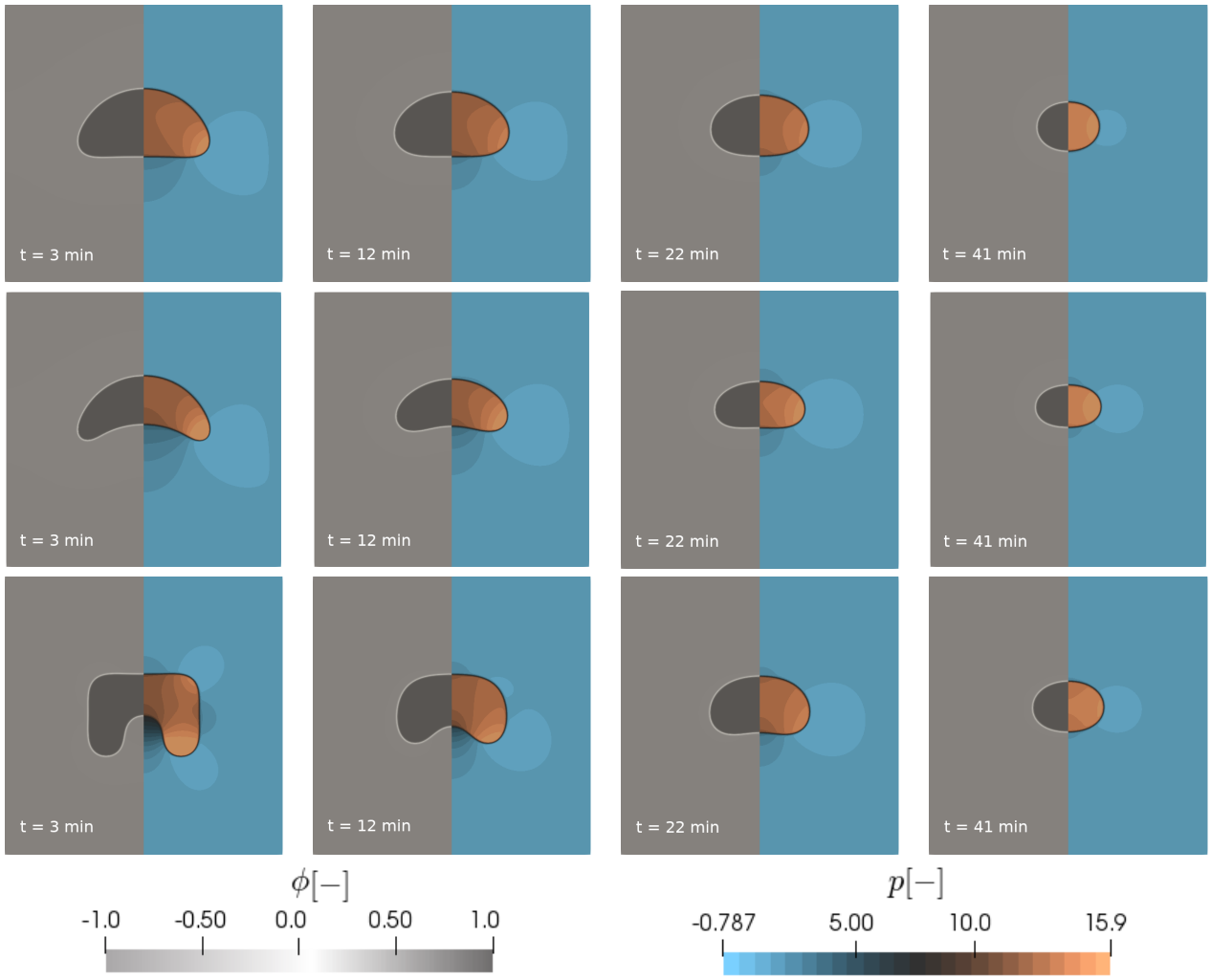

Figure 3: Numerical time lapses of gap closure for each of the three distinct initial wound shapes: *half circle* (first row), *half moon* (second row) and *square inset* (third row). The left side of each figure shows the wound profile, while the right side shows the pressure profile.

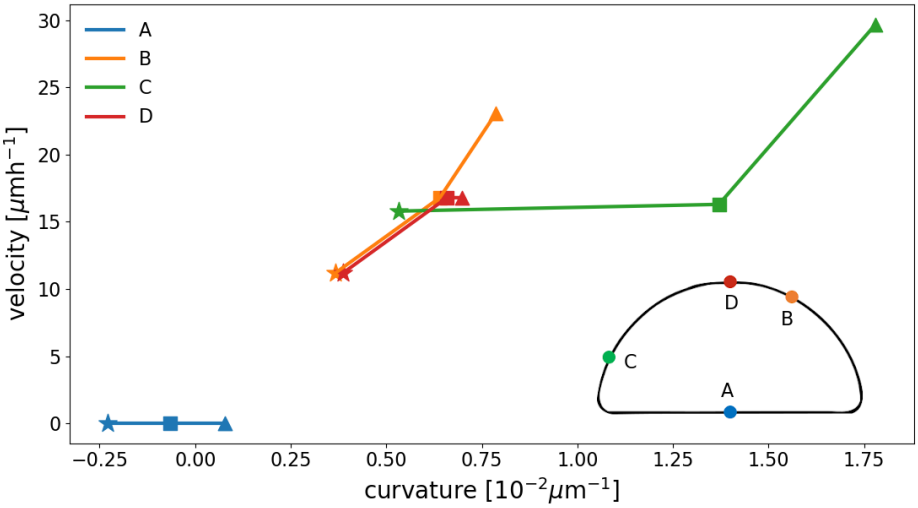

Figure 4: Plot of the normal velocity versus the local curvature for different interface points $A - D$ initially shown in the *half circle* geometry. For every point, *velocity-curvature* pairs are extracted at the time 0 min (star marker), 6 min (square marker) , 18 min (triangle marker). We remark that the curvature was estimated from the chemical potential μ basing on the formulas obtained in the asymptotic limit rather than directly computed from the geometry.

wound, as shown in Fig.5. The wound area decreases in a near-linear manner over time up to the complete closure regardless of the initial shape of the gap. A comparison between the numerical results and the experimental data extracted from [19] for each of the considered gap geometries is also shown in Fig.5. In order to achieve a deeper understanding of the system behavior, we investigate the influence of the dimensionless parameters on the model response for square inset geometry. In Fig. S1 (Supplementary Information) , we notice that lower crawling, i.e. decreasing the value for the dimensionless term $\bar{\Gamma}$, is correlated with longer healing times. The same behavior is observed also for the dimensionless motility $\bar{M}$, so that reducing the friction with the substrate increases the velocity of gap closure. We also observe that decreasing Da not only speeds up the closure process, but creates swirling patterns in the normal velocity field surrounding the wound, as shown in Fig. S2 (Supplementary Information), similar to the ones observed in other system models [29].

Finally, we explore the effect the crawling on the closure dynamics given by the dimensionless parameters $\bar{f_L}$ and $\bar{\Gamma}$ in determining the dynamics of gap closure. We find that $\bar{f_L}$ acts as an extra pressure term in $\bar{p}$, not affecting directly the healing time and the shape evolution, that are indeed controlled by $\bar{\Gamma}$, as discussed earlier.

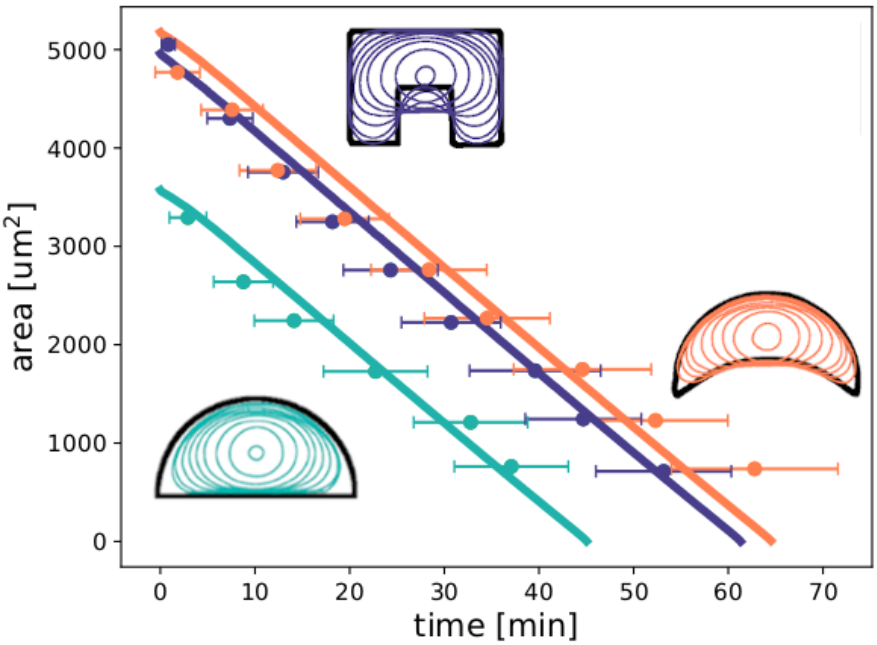

Figure 5: In-silico simulated decrease of the area over time for three differently shaped wounds: *square inset* (blue line), *half circle* (green line) and *half moon* (orange line) with initial area of $3500 - 5000\,\mu m^2$. The horizontal bars coincides with the error bars of the experimental data extracted from [19] for each geometry. The image shows also the overlay of outlines at different time points for each of the three wound shapes.

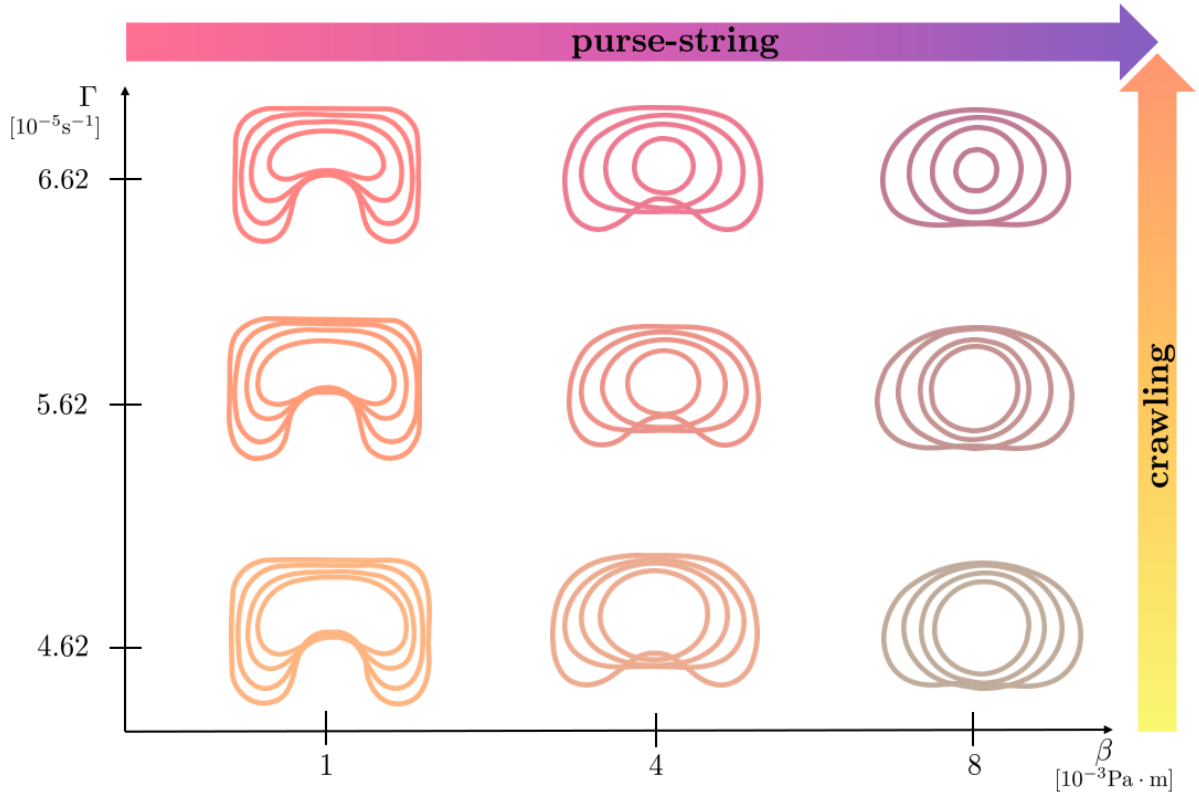

Figure 6: Phase diagram describing the evolution of the wound edge (square inset geometry) during the closure process by varying the purse-string intensity β and the crawling rate Γ. Each figure is obtained by overlapping the simulated wound edges at time $t \simeq 12\,\text{min}$, $24\,\text{min}$, $36\,\text{min}$, $48\,\text{min}$.

In Fig. 6, we report the resulting morphological diagrams of the closing dynamics by exploring different combinations between the crawling and the purse string dimensional parameters. We notice that an increase of the purse-string force results into a regularization of the wound shapes at the same time instants, i.e. the wound protrusions into the healthy tissue tend to disappear early during the healing process. On the other hand, an increase of the crawling rate accelerates closing by preserving the initial morphology of the wound against the regularizing effect of the purse-string mechanism. In Fig. 7, we depict the morphological changes at given time instants by varying one of such parameters at the time, thus to highlight the different geometrical effects.

Finally, we plot the principal stress pattern σ_{max} for the *square inset* geometry. We observe that in the early stages of the healing process, regions in proximity of convex border are characterized by a compressive stress pattern indicating that the cell crawling contribution is suppressed by the actomyosin

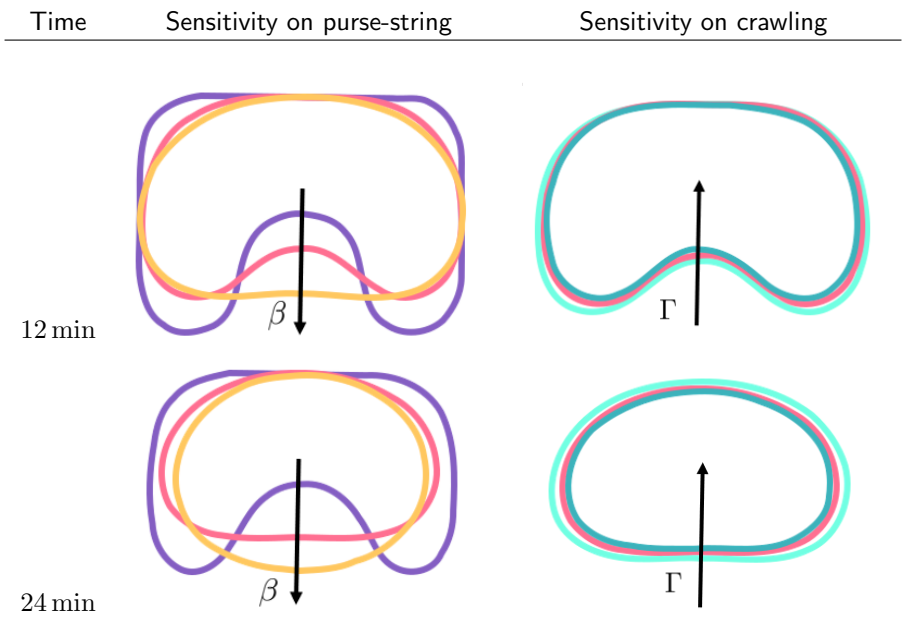

Figure 7: Overlap of the wound profiles for different purse-string intensities (left column) and for different crawling intensities (right column) at time $t = 12\,\mathrm{min}$ (first row) and $t = 24\,\mathrm{min}$ (second row). Black arrows indicate the direction of the parameter increase. On the left, we set $\Gamma = 5.62 \cdot 10^{-5}\,\mathrm{s}^{-1}$ and we vary $\beta = \{1,\ 4,\ 8\ \} \cdot\ 10^{-3}\,\mathrm{Pa\,m}$; on the right, we set $\beta = 4 \cdot 10^{-3}\,\mathrm{Pa\,m}$ and we vary $\Gamma = \{4.62,\ 5.62,\ 6.62\ \} \cdot 10^{-5}\,\mathrm{s}^{-1}$.

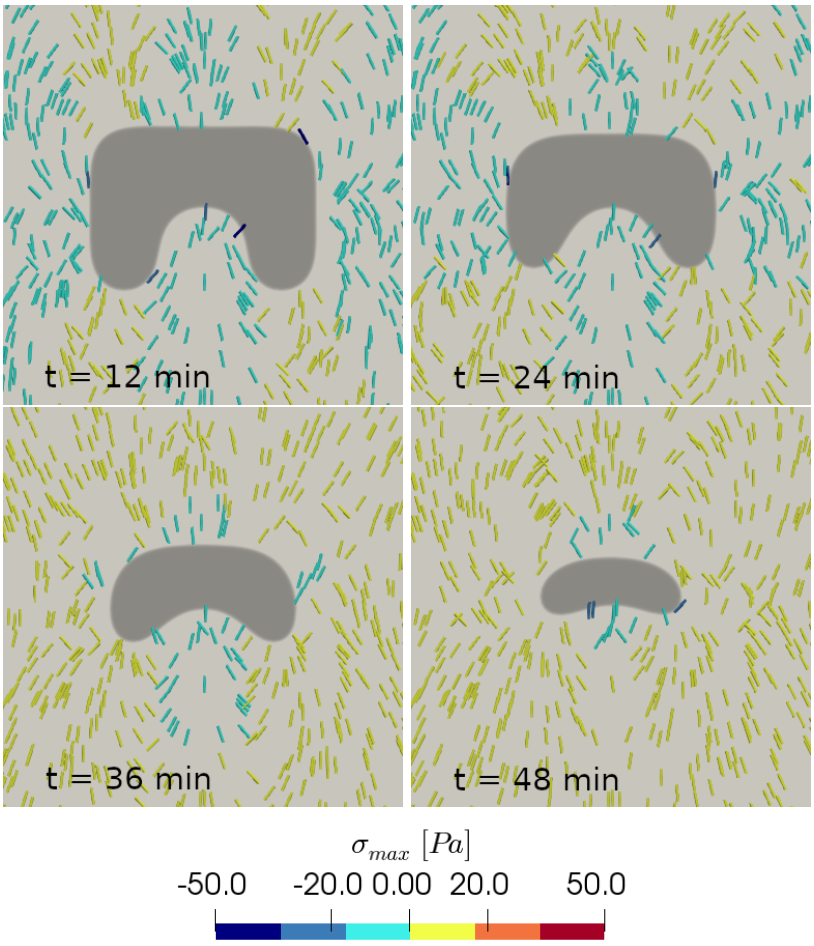

Figure 8: Vectorial map of the principal stress at different time instants of the closing process for the *square inset* geometry in a crawling-dominant scenario. The set of parameters used is $\beta = 1 \cdot 10^{-3}\,\mathrm{Pa\,m}$ and $\Gamma = 6.62 \cdot 10^{-5}\,\mathrm{s}^{-1}$. The colormap describes the stress intensity.

cable action. In contrast, areas in the vicinity of concave borders present a traction stress pattern. In later stages, when the wound evolves towards more regular shapes, with concave borders almost everywhere, the traction pattern becomes the dominant one (Fig. 8). These results are in good qualitative agreement with the traction force microscopy measurements presented in [17], showing force components that are both radial and tangential to the wound for the effect of the substrate friction.

Discussion

In this work we present a novel diffuse interface model to characterize mechano-biological features during epithelial closure. The model is derived by thermo-dynamical principles within the mixture theory framework. We considered a viscous mixture behaving as a Darcy-Brinkman-Korteweg fluid with volumetric mass sources and a diffusive mass flux. The diffusive mass flux follows the gradient flow of a chemical potential μ, containing a local interaction term that acts as an active surface tension, mimicking the active purse-string mechanisms, and a regularising short-range nonlocal interaction that controls the width of the interface. The crawling of the lamellipodia appears as the combined effect of an extra-pressure in the chemical potential and a crawling rate Γ in the Cahn-Hilliard equation.

We performed an asymptotic analysis obstaining the sharp interface limit of our model, in order to investigate the role of interfacial forces and of the frictional forces with the substrate in governing the wound edge movements. We found that the Korteweg forces driven by the diffusive chemical potential and the crawling impose a pressure jump across the interface. Moreover, the diffusion of the chemical potential is governed by a Mullins-Sekerka system, and its interfacial value is given by a Gibbs-Thompson relation driven by the purse-string tension, and a Stefan law driven by the frictional forces.

The model has been finally numerically approximated using a Finite Element discretization. We found that our *in-silico* numerical results are in good quantitative agreement with the *in-vitro* experiments reported in [19]. The quasi-linear trend in the decrease of the area over time is confirmed and the numerical closure time is aligned with the experimental one for all the considered gap geometries. We also found a similar morphological evolution of the wound edge during the closing dynamics. In particular, we observed a local regulation of the closure mechanism governed by the curvature of the gap edge: curved regions move at a significantly higher velocity than that of flat edges, thus resulting in a change of the gap geometry during the tissue repair process. Indeed, during the first stages of the process, the wound evolves towards a more regular shape up to form an elliptic or circular hole. Afterwards, the gap closes symmetrically with homogeneous velocity till the end of the closure process.

Our sharp interface limit is a supporting evidence that the curvature of the edge has a major role in regulating the closure mechanism. Indeed, we showed that the local curvature affects the pressure jump at the border and tunes the direction of the purse-string force. In regions where the edge is positively curved the force is directed towards the inner of the wound; on contrary, the purse-string action is oriented

towards the healthy tissue when the curvature is negative. Thereby, our diffuse interface model is able to capture the observed gap closure dynamics dictated by the presence of the actomyosin cable. Its numerical implementation is finally robust and computationally much more affordable compared to the its sharp interface counterpart.

In conclusion, this work sheds light on the geometric control by active mechanics during the epithelial closure dynamics. Compared to existing sharp interface approaches, the use of a diffuse interface significantly reduces the numerical complexities related to the need to track the border movements and to impose jump conditions on the forces across the free boundary. In our model, the active mechanical features around the edge curvature are instead naturally embedded into the bulk equations as Korteweg forces. The numerical results not only quantitatively predict the universal quasi-linear decrease of area over time and the observed morphological transitions of the wound edge, but also qualitatively agree with the traction force patterns reported in existing experiments, highlighting the interplay between edge and frictional forces.

However, we remark that our diffuse interface approach suffers some limitations that require future developments. In particular, we plan to improve the current model by developing a chemo-mechanical coupling between the fast dynamics of calcium waves and myosin activation that trigger the purse-string and crawling forces during the closure dynamics. Finally, as a further next step of our work, we aim at exploring different systems models to give a quantitative comparison of the numerical predictions against a traction force microscopy measurements with varying adhesive properties with the substrate.

Conflicts of Interest

There are no conflicts of interest to declare.

Acknowledgements

This project was supported by GNFM – INdAM through the program Progetto Giovani 2023, and by MUR through both the PRIN Research Project 2020F3NCPX and the grant Dipartimento di Eccellenza 2023-2027.

References

[1] K. J. Sonnemann and W. M. Bement. "Wound repair: toward understanding and integration of single-cell and multicellular wound responses." In: *Annual review of cell and developmental biology* 27 (2011), pp. 237–263.

[2] J. D. Murray. *Mathematical biology II: spatial models and biomedical applications*. Vol. 3. Springer New York, 2001.

[3] H A S van den Brenk. "Studies in restorative growth processes in mammalian wound healing." In: *British Journal of Surgery* 43.181 (Dec. 2005), pp. 525–550. eprint: `https://academic.oup.com/bjs/article-pdf/43/181/525/37395011/bjs18004318115.pdf`.

[4] J. A. Sherratt and J. D. Murray. "Models of epidermal wound healing." In: *Proceedings of the Royal Society of London. Series B: Biological Sciences* 241.1300 (1990), pp. 29–36.

[5] J. A. Sherratt. "Mathematical models of wound healing." PhD thesis. University of Oxford, 1991.

[6] J. A. Sherratt and J. D. Murray. "Article Commentary: Epidermal Wound Healing: The Clinical Implications of a Simple Mathematical Model." In: *Cell Transplantation* 1.5 (1992), pp. 365–371.

[7] T. T. Irvin. "The healing wound." In: *Wound healing for surgeons* (1984), pp. 3–28.

[8] R. A. F. Clark. "Wound repair." In: *The molecular and cellular biology of wound repair* (1988), pp. 3–50.

[9] P. Martin and J. Lewis. "Actin cables and epidermal movement in embryonic wound healing." In: *Nature* 360.6400 (1992), pp. 179–183.

[10] G. Fenteany, P. A. Janmey, and T. P. Stossel. "Signaling pathways and cell mechanics involved in wound closure by epithelial cell sheets." In: *Current Biology* 10.14 (2000), pp. 831–838.

[11] B. G. Fernández, A. M. Arias, and A. Jacinto. "Dpp signalling orchestrates dorsal closure by regulating cell shape changes both in the amnioserosa and in the epidermis." In: *Mechanisms of development* 124.11-12 (2007), pp. 884–897.

[12] M. T. Abreu-Blanco et al. "Drosophila embryos close epithelial wounds using a combination of cellular protrusions and an actomyosin purse string." In: *Journal of cell science* 125.24 (2012), pp. 5984–5997.

[13] S. Begnaud et al. “Mechanics of epithelial tissues during gap closure.” In: *Current opinion in cell biology* 42 (2016), pp. 52–62.

[14] K. E. Rothenberg and R. Fernandez-Gonzalez. “Forceful closure: cytoskeletal networks in embryonic wound repair.” In: *Molecular biology of the cell* 30.12 (2019), pp. 1353–1358.

[15] E. Anon et al. “Cell crawling mediates collective cell migration to close undamaged epithelial gaps.” In: *Proceedings of the National Academy of Sciences* 109.27 (2012), pp. 10891–10896.

[16] V Nier et al. “Tissue fusion over nonadhering surfaces.” In: *Proceedings of the National Academy of Sciences* 112.31 (2015), pp. 9546–9551.

[17] A. Brugués et al. “Forces driving epithelial wound healing.” In: *Nature physics* 10.9 (2014), pp. 683–690.

[18] S Vedula et al. “Mechanics of epithelial closure over non-adherent environments.” In: *Nature Communications* 6.1 (2015), p. 6111.

[19] A. Ravasio et al. “Gap geometry dictates epithelial closure efficiency.” In: *Nature communications* 6.1 (2015), pp. 1–13.

[20] T. Chen et al. “Large-scale curvature sensing by directional actin flow drives cellular migration mode switching.” In: *Nature physics* 15.4 (2019), pp. 393–402.

[21] V. Ajeti et al. “Wound healing coordinates actin architectures to regulate mechanical work.” In: *Nature physics* 15.7 (2019), pp. 696–705.

[22] E. Javierre et al. “A mathematical analysis of physiological and morphological aspects of wound closure.” In: *Journal of mathematical biology* 59.5 (2009), pp. 605–630.

[23] A. Sadovsky and F. Y. M. Wan. “The elastodynamics of embryonic epidermal wound closure.” In: *Studies in Applied Mathematics* 118.4 (2007), pp. 365–395.

[24] P. Lee and C. W. Wolgemuth. “Crawling cells can close wounds without purse strings or signaling.” In: *PLoS computational biology* 7.3 (2011).

[25] J. C. Arciero et al. “Continuum model of collective cell migration in wound healing and colony expansion.” In: *Biophysical journal* 100.3 (2011), pp. 535–543.

[26] J. C. Arciero et al. “Using a continuum model to predict closure time of gaps in intestinal epithelial cell layers.” In: *Wound Repair and Regeneration* 21.2 (2013), pp. 256–265.

[27] B. Li et al. "EML webinar overview: Dynamics of collective cells." In: *Extreme Mechanics Letters* 44 (2021), p. 101255.

[28] S.-Z. Lin et al. "Universal statistical laws for the velocities of collective migrating cells." In: *Advanced Biosystems* 4.8 (2020), p. 2000065.

[29] S.-Z. Lin et al. "Collective dynamics of coherent motile cells on curved surfaces." In: *Soft Matter* 16.12 (2020), pp. 2941–2952.

[30] Filippos Ioannou et al. "Development of a new 3D hybrid model for epithelia morphogenesis." In: *Frontiers in Bioengineering and Biotechnology* 8 (2020), p. 405.

[31] S. Najem and M. Grant. "Phase-field model for collective cell migration." In: *Physical Review E* 93.5 (2016), p. 052405.

[32] B. Palmieri et al. "Multiple scale model for cell migration in monolayers: Elastic mismatch between cells enhances motility." In: *Scientific reports* 5.1 (2015), p. 11745.

[33] Adrian Moure and Hector Gomez. "Phase-field modeling of individual and collective cell migration." In: *Archives of Computational Methods in Engineering* 28 (2021), pp. 311–344.

[34] M. Antunes et al. "Coordinated waves of actomyosin flow and apical cell constriction immediately after wounding." In: *Journal of Cell Biology* 202.2 (2013), pp. 365–379.

[35] D. Lee et al. "Physical, mathematical, and numerical derivations of the Cahn–Hilliard equation." In: *Computational Materials Science* 81 (2014), pp. 216–225.

[36] A. Agosti et al. "A computational framework for the personalized clinical treatment of glioblastoma multiforme." In: *ZAMM-Journal of Applied Mathematics and Mechanics/Zeitschrift für Angewandte Mathematik und Mechanik* 98.12 (2018), pp. 2307–2327.

[37] M. Doi. *Soft matter physics*. Oxford University Press, 2013.

[38] M. Ebenbeck, H. Garcke, and R. Nürnberg. "Cahn–Hilliard–Brinkman systems for tumour growth." In: *Discrete and Continuous Dynamical Systems-S* 14.11 (2021), pp. 3989–4033.

[39] J. Lowengrub and L. Truskinovsky. "Quasi–incompressible Cahn–Hilliard fluids and topological transitions." In: *Proceedings of the Royal Society of London. Series A: Mathematical, Physical and Engineering Sciences* 454.1978 (1998), pp. 2617–2654.

[40] A. A. Lee, A. Munch, and E. Suli. "Sharp-Interface limits of the Cahn–Hilliard equation with degenerate mobility." In: *SIAM Journal on Applied Mathematics* 76.2 (2016), pp. 433–456.

[41] H. Garcke et al. "A Cahn–Hilliard–Darcy model for tumour growth with chemotaxis and active transport." In: *Mathematical Models and Methods in Applied Sciences* 26.06 (2016), pp. 1095–1148.

[42] W. Dreyer and B. A. Wagner. "Sharp-interface model for eutectic alloys. Part I: Concentration dependent surface tension." In: *Interfaces and Free Boundaries* 7.2 (2005), pp. 199–227.

[43] P. C. Fife and O. Penrose. "Interfacial dynamics for thermodynamically consistent phase-field models with nonconserved order parameter." In: (1995).

[44] M. S. Alnæs et al. *The FEniCS project version 1.5. Arch. Numer. Softw. 3.* 2015.

[45] A. Logg, G. N. Wells, and J. Hake. "DOLFIN: A C++/Python finite element library." In: *Automated solution of differential equations by the finite element method.* Springer, 2012, pp. 173–225.

[46] C. Blanch-Mercader et al. "Effective viscosity and dynamics of spreading epithelia: a solvable model." In: *Soft Matter* 13.6 (2017), pp. 1235–1243.

MOX Technical Reports, last issues

Dipartimento di Matematica
Politecnico di Milano, Via Bonardi 9 - 20133 Milano (Italy)

81/2023 Buchwald, S.; Ciaramella, G; Salomon, J.; Sugny, D.
A SPIRED code for the reconstruction of spin distribution

79/2023 Agosti, A.; Bardin, R.; Ciarletta, P.; Grasselli, M.
A diffuse interface model of tumour evolution under a finite elastic confinement

78/2023 Antonietti, P.F.; Bonizzoni, F.; Corti, M.; Dall'Olio, A.
Discontinuous Galerkin for the heterodimer model of prion dynamics in Parkinson's disease

77/2023 Fumagalli, I.; Corti, M.; Parolini, N.; Antonietti, P. F.
Polytopal discontinuous Galerkin discretization of brain multiphysics flow dynamics

76/2023 Ieva, F.; Galliani, G.; Secchi, P.
The impact of public transport on the diffusion of COVID-19 pandemie in Lombardy during 2020

74/2023 Pidò, S.; Pinoli, P.; Crovari, P.; Ieva, F.; Garzotto, F.; Ceri, S.
Ask Your Data—Supporting Data Science Processes by Combining AutoML and Conversational Interfaces

75/2023 Archetti, A.; Ieva, F.; Matteucci, M.
Scaling survival analysis in healthcare with federated survival forests: A comparative study on heart failure and breast cancer genomics

71/2023 Conni, G.; Piccardo, S.; Perotto, S.; Porta, G.M.; Icardi, M.
HiPhome: HIgh order Projection-based HOMogEnisation for advection diffusion reaction problems

70/2023 Ragni, A.; Ippolito, D.; Masci, C.
Assessing the Impact of Hybrid Teaching on Students' Academic Performance via Multilevel Propensity Score-based techniques

69/2023 Ferro, N.; Micheletti, S.; Parolini, N.; Perotto, S.; Verani, M.; Antonietti, P. F.
Level set-fitted polytopal meshes with application to structural topology optimization